Four-Button BPM Coefficients in Cylindrical and Elliptic Beam Chambers

S. H. Kim
February 17, 1999

Beam position monitor (BPM) coefficients are calculated from induced charges on four-button BPMs in circular and elliptic beam chambers for $\gamma >> 1$. Since the beam chamber cross-section for the APS storage ring is different from an exact elliptic geometry, numerical values of the BPM coefficients and their inversions are computed from two-dimensional electrostatic field distributions inside an exact geometry of the beam chamber. Utilizing Green's reciprocation theorem, a potential value is applied to the buttons rather than changing the beam position, and potential distributions corresponding to the beam positions are then computed.

1. Cylindrical Chamber

A charged particle beam of short bunches induces charges on the beam chamber wall. Due to the Lorentz contraction, for $\gamma >> 1$, where γ is the relativistic factor, these charges have the same longitudinal intensity modulation as the beam. The electromagnetic fields associated with the beam are obtained by the Lorentz transformation from the fixed lab frame F to a moving reference frame F', where the charged beam is at rest [1, 2]. The field distribution inside the beam chamber becomes an electrostatic problem in the moving reference frame. Here we assume that the buttons are installed flush with the inner surface of the beam chamber, with the chamber having constant cross-section and the chamber wall at a uniform potential.

For the charge density of a filament beam located at (x_o, y_o) in the transverse plane of the Cartesian coordinates and moving with a wave number k in the longitudinal direction z in the lab frame F,

$$\rho = \rho_k(x_o, y_o)\cos k(z - vt); \tag{1}$$

the charge density in the reference frame F', in which the beam is at rest, is expressed as

$$\rho' = \frac{\rho_k(x_o, y_o)}{\gamma}\cos(kz'/\gamma). \tag{2}$$

For the filament beam of Eq. (2) located at (r_o, θ_o) in the cylindrical coordinates, the Poisson's equation is

$$\left\{\frac{1}{r}\frac{\partial}{\partial r}(r\frac{\partial}{\partial r}) + \frac{1}{r^2}\frac{\partial^2}{\partial\theta^2} - \frac{k^2}{\gamma^2}\right\}\phi = -\frac{\rho'}{\varepsilon_o}. \tag{3}$$

The solution for the electrostatic potential is a form of the Bessel function with an argument of kr/γ. When $k/\gamma \to 0$ and $\phi(a,\theta) = 0$, the potential for $r > r_o$ is given by

$$\phi(r,\theta) = -\frac{\rho_k}{2\pi\varepsilon_o\gamma}\cos(kz'/\gamma)[\ln(\frac{r}{a}) - \sum_{n=1}^{\infty}\frac{1}{n}\{(\frac{r_o}{r})^n - (\frac{rr_o}{a^2})^n\}\cos n(\theta - \theta_o)]. \tag{4}$$

The surface charge density induced per unit length on the inner surface of the chamber in the longitudinal direction is calculated from Eq. (4) in the lab frame F

$$\sigma(a,\theta) = -\frac{\rho_k}{2\pi a}\cos k(z-vt)[1+2\sum_{n=1}^{\infty} (\frac{r_o}{a})^n \cos n(\theta-\theta_o)], \tag{5}$$

where $1/\gamma$ is cancelled from the relation $E_\perp = \gamma E'_\perp$. Assuming the BPM coefficients are not depend on cos $k(z\text{-}vt)$, that factor is omitted in the following expressions. The induced charges associated with the sum, vertical, and horizontal signals for four-button BPMs, shown in Fig. 1(a), are therefore given by

$$Q_s = -\rho_k \frac{4\Delta\theta}{2\pi}[1+\sum_{n=1}^{\infty}\{1+(-1)^n\}(\frac{r_o}{a})^n \cos n\theta_p \cos n\theta_o (\frac{\sin n\Delta\theta/2}{n\Delta\theta/2})],$$

$$Q_y = -\rho_k \frac{4\Delta\theta}{2\pi}\sum_{n=1}^{\infty}\{1-(-1)^n\}(\frac{r_o}{a})^n \sin n\theta_p \sin n\theta_o (\frac{\sin n\Delta\theta/2}{n\Delta\theta/2}), \tag{6}$$

$$Q_x = -\rho_k \frac{4\Delta\theta}{2\pi}\sum_{n=1}^{\infty}\{1-(-1)^n\}(\frac{r_o}{a})^n \cos n\theta_p \cos n\theta_o (\frac{\sin n\Delta\theta/2}{n\Delta\theta/2}).$$

2. Elliptic Chamber

The Poisson's equation in the Cartesian coordinates, $\nabla^2\phi = -\rho'/\varepsilon_o$, for the filament beam of Eq. (2) may be written as

$$[\frac{\partial^2}{\partial x^2}+\frac{\partial^2}{\partial y^2}-\frac{k^2}{\gamma^2}]G(x,y;x_o,y_o) = -\delta(x-x_o)\delta(y-y_o), \tag{7}$$

where $G(x,y;x_o,y_o)$ is a Green's function to be solved, and the electrostatic potential in the lab frame can be calculated from the Green's function

$$\phi = \iint dx_o dy_o \frac{\rho_k(x_o,y_o)}{\varepsilon_o\gamma}\cos k(z-vt)G(x,y;x_o,y_o). \tag{8}$$

For a beam chamber of elliptic cross-section, the following inverse hyperbolic cosine transformation makes it possible to solve Eq. (7) analytically:

$$w = u + i\theta = \cosh^{-1}(z/d),$$

or $$z = x + i\,y = d\,(\cosh u \cos\theta + i \sinh u \sin\theta) \tag{9}$$

with $$h_u = h_\theta = |dz/dw| = d(\cosh^2 u - \cos^2\theta)^{1/2}.$$

Then, for a constant u_c,

$$(\frac{x}{d\cosh u_c})^2 + (\frac{y}{d\sinh u_c})^2 = 1 \tag{10}$$

represents a confocal ellipse with foci at $\pm\, d$, and similarly, constant values of θ make a set of confocal hyperbolas orthogonal to the ellipse as shown in Fig. 1(b). Table 1 lists the parameters for the synchrotron and storage ring chambers before and after the transformation.

Table 1. Beam Chamber Parameters with Units in mm

Synchrotron	major axis=30	minor axis=18.5	u_c = 0.7196	d = 23.62
Storage Ring	42.34	20.85	0.5393	36.85

After the elliptic transformation, Eq. (7) becomes

$$[\frac{\partial^2}{\partial u^2} + \frac{\partial^2}{\partial \theta^2} - \frac{k^2 d^2}{\gamma^2}(\cosh^2 u - \cos^2\theta)]G(u,\theta;u_o,\theta_o) = -\delta(u-u_o)\delta(\theta-\theta_o), \tag{11}$$

and

$$\phi(u,\theta) = \int_0^{u_c}\int_0^{2\pi} \frac{\rho_k(u_o,\theta_o)}{\varepsilon_o \gamma}\cos k(z-vt) G(u,\theta;u_o,\theta_o) d\theta_o du_o. \tag{12}$$

Equation (11) may be separated into two Mathieu equations. After Laplace transformations, radial solutions are obtained as a series of Bessel and Neumann functions with arguments of $kd/\gamma \cosh u$ and $kd/\gamma \cos\,\theta$. For $kd/\gamma \ll 1$, it is not worthwhile to perform the task of calculating an exact solution and then approximate it in order to compute numerical values [3]. Instead, kd/γ is set to zero in Eq. (11) and solved with boundary conditions of $\phi(\mu_c,\theta) = 0$ and $\phi(0,\theta)$ = continuous. Then, the Green's functions are given by

$$G(u,\theta;u_o,\theta_o) = -\frac{u_o - u_c}{2\pi} - \frac{1}{\pi}\sum_{m=1}^{\infty}\frac{1}{m}e^{-mu_c}\,[\{\frac{\cosh mu_o}{\cosh mu_c} - e^{-m(u_o-u_c)}\}\cosh mu \cos m\theta_o \cos m\theta$$
$$+\{\frac{\sinh mu_o}{\sinh mu_c} - e^{-m(u_o-u_c)}\}\sinh mu \sin m\theta_o \sin m\theta, \qquad (u \le u_o) \tag{13}$$

and

$$G(u,\theta;u_o,\theta_o) = -\frac{u - u_c}{2\pi} - \frac{1}{\pi}\sum_{m=1}^{\infty}\frac{1}{m}e^{-mu_c}\,[\cosh mu_o\{\frac{\cosh mu}{\cosh mu_c} - e^{-m(u-u_c)}\}\cos m\theta_o \cos m\theta$$
$$+\sinh mu_o\{\frac{\sinh mu}{\sinh mu_c} - e^{-m(u-u_c)}\}\sin m\theta_o \sin m\theta. \qquad (u \ge u_o) \tag{14}$$

Because of the boundary condition that ϕ be continuous near u = 0, there are no terms such as $\cosh(mu)\sin(m\theta)$ and $\sinh(mu)\cos(m\theta)$ in Eqs. (13) and (14). Since the curves with constant values of θ are orthogonal with the chamber surface, $u = u_c$, the induced charge density on the chamber surface $\sigma(u_c,\theta) = -\,\varepsilon_o(\partial\phi/\partial u)$ at u=u_c is calculated from Eqs. (12) and (14) as

$$\sigma(u_c,\theta) = -\frac{\rho_k}{2\pi}[1+2\sum_{m=1}^{\infty}(\frac{\cosh mu_0}{\cosh mu_c}\cos m\theta_o \cos m\theta + \frac{\sinh mu_0}{\sinh mu_c}\sin m\theta_o \sin m\theta)]. \qquad (15)$$

As in the case of the cylindrical chamber, the cos $k(z\text{-}vt)$ factor is omitted in the following expressions. The induced charges associated with the sum (Q_s), vertical (Q_y), and horizontal (Q_x) signals for four-button BPMs shown in Fig. 1(b) are given by

$$Q_s = -\rho_k \frac{4\Delta\theta}{2\pi}[1+\sum_{m=1}^{\infty}\{1+(-1)^m\}\frac{\cosh mu_0}{\cosh mu_c}\cos m\theta_o \cos m\theta_p (\frac{\sin m\Delta\theta/2}{m\Delta\theta/2})], \qquad (16)$$

$$Q_y = -\rho_k \frac{4\Delta\theta}{2\pi}\sum_{m=1}^{\infty}\{1-(-1)^m\}\frac{\sinh mu_0}{\sinh mu_c}\sin m\theta_o \sin m\theta_p (\frac{\sin m\Delta\theta/2}{m\Delta\theta/2}), \qquad (17)$$

$$Q_x = -\rho_k \frac{4\Delta\theta}{2\pi}\sum_{m=1}^{\infty}\{1-(-1)^m\}\frac{\cosh mu_0}{\cosh mu_c}\cos m\theta_o \cos m\theta_p (\frac{\sin m\Delta\theta/2}{m\Delta\theta/2}). \qquad (18)$$

3. Numerical Values of the BPM Coefficients

Numerical values of the BPM coefficients and their inversions are computed from two-dimensional electrostatic field distribution inside an exact geometry of the beam chamber. The last three equations were used only to cross check the computation results. Figure 2 shows the cross-section of the beam chamber. The four 10-mm-diameter buttons are installed symmetrically with respect to the origin of the coordinates at (x_o, y_o) = (±14.0 mm, ±19.0 mm), flush with the chamber surface.

When +1.0 V is applied to all four buttons and the conducting chamber is grounded, the potential at any point in the chamber is defined as the sum signal Q_s. In Fig. 2 there are 20 equipotential lines between a button and the chamber. The potential near the origin is between 0.25 and 0.3 V. The potential at (5, 5), for example, is 0.302 V. Having Q_s = 0.302 C in Eq. (16) with ρ_k = –0.95 C/mm^2 yields equivalent results. Since we are only concerned with the relative magnitudes of the sum, vertical, and horizontal signals, the signal units will now be ignored.

The equipotential contours for the vertical and horizontal signals are shown in Fig. 3. The vertical signal Q_y was obtained by applying +1V to the upper two buttons and –1V to the lower two buttons. Similarly, the horizontal signal Q_x was obtained by applying +1V to the right two buttons and –1V to the left two buttons. Asymmetry of the signal (due to the antechamber) is relatively small. At y_o = 5 mm, the vertical signal difference for x_o = ± 10 mm is less than 10^{-3}, and that for x_o = ±15 mm is 5×10^{-3}. At y_o = 0, the horizontal signal difference for a given ± x_o is less than 2.5×10^{-3}.

Vertical and sum signals vs the vertical beam position y_o are plotted in Fig. 4 at selected horizontal beam position x_o. Higher sensitivities of the signals for $|y_o|$ > 10 mm at x_o = 15 mm, for example, are seen from the contour plots of Figs. 2 and 3. Fortunately, the normalized vertical signals (Q_y/Q_s), plotted in Fig. 5, are closer to linear variations with respect to the vertical beam positions. The normalized signals are also plotted as a function of the horizontal beam positions in Fig. 5.

Similarly, horizontal, sum, and normalized horizontal (Q_x/Q_s) signals are plotted in Figs. 6 and 7. Relatively large variations of Q_x and Q_s at y_o = 15 mm are expected from the contour plots of Figs. 2 and 3. The variations of the normalized signals are smoother. However, their sensitivities are severely reduced for $|x_o| > 10$ mm.

In Table 2, coefficients for polynomial curve fits are listed for the normalized vertical signals (Q_y/Q_s) vs the vertical beam positions y_o and their inversions at selected horizontal beam positions. Ideally, the coefficients of even orders should be zero; small values are due to the antechamber and computation errors. Within $|y_o| < 15$ mm, as the R-values indicate the reliability of the curve fits, third-order polynomial seems to be good enough. In the last row, the coefficients for linear fits within $|y_o| < 5$ mm are listed.

The coefficients for the normalized horizontal signals are listed in Table 3. The horizontal beam positions are limited to $|x_o| < 15$ mm for $y_o = 0$ and 5 mm, and $|x_o| < 10$ mm for $y_o = 10$ and 15 mm.

References

[1] J. H. Cuperus, "Monitoring of Particle Beams at High Frequencies," *Nucl. Instrum. Methods*, **145**, 219 (1977).

[2] S. Krinsky, "Measurement of the Longitudinal Parameters of an Electron Beam in a Storage Ring," Lecture Notes in Phys. 343, M. Month and S. Turner (Eds.), Springer-Verlag (1989), p. 150.

[3] P. Morse and H. Feshbach, *Methods of Theoretical Physics*, Chapters 5 and 11, McGraw-Hill (1953).

Table 2. Polynomial coefficients for Q_y/Q_s vs y_o ($|y_o|$ < 15 mm) and their inversions up to the fifth and third orders at selected values of x_o. R-values indicate the reliability of the curve fits. The linear coefficients within $|y_o|$ < 5 mm are listed in the last row.

(a) $V = M_o + M_1 y_o + M_2 y_o^2 + \cdots + M_5 y_o^5$, ($V = Q_y/Q_s$)					
	$x_o = 0$	$x_o = 5$	$x_o = 10$	$x_o = 15$	$x_o = 20$
M_o	-1.52E-06	8.56E-05	0.0003699	0.0008404	0.0013309
M_1	0.055024	0.059777	0.069485	0.074561	0.069003
M_2	7.29E-09	-3.11E-06	-4.23E-06	-3.32E-06	-1.95E-06
M_3	-6.14E-05	-5.22E-05	-4.59E-05	-4.36E-05	-3.69E-05
M_4	-4.04E-11	1.38E-09	7.99E-09	1.01E-09	1.68E-09
M_5	3.37E-08	2.30E-08	-1.69E-08	-6.13E-08	-3.02E-08
R	1	1	1	1	1
(b) $V = M_o + M_1 y_o + M_2 y_o^2 + M_3 y_o^3$					
M_o	-1.52E-06	7.94E-05	0.000334	0.0008359	0.0013234
M_1	0.055024	0.05949	0.069696	0.075324	0.069378
M_2	7.29E-09	-2.84E-06	-2.66E-06	-3.13E-06	-1.62E-06
M_3	-6.14E-05	-4.64E-05	-5.02E-05	-5.92E-05	-4.45E-05
R	1	1	1	0.99999	1
(c) $y_o = m_o + m_1 V + m_2 V^2 + \cdots + m_5 V^5$, **(Inverted polynomial coefficients)**					
	$x_o = 0$	$x_o = 5$	$x_o = 10$	$x_o = 15$	$x_o = 20$
m_o	3.01E-05	-0.001185	-0.005304	-0.011073	-0.019332
m_1	18.412	16.828	14.521	13.633	14.603
m_2	-0.000107	0.0054239	0.0098128	0.0011322	0.0011304
m_3	2.5812	2.7239	0.75408	-0.36652	0.608
m_4	0.0004878	0.048948	0.00424	0.0069947	-0.009774
m_5	21.593	6.6561	3.3942	3.7815	2.8276
R	1	1	1	0.99999	1
(d) $y_o = m_o + m_1 V + m_2 V^2 + m_3 V^3$					
m_o	2.30E-05	-0.002415	-0.005465	-0.011718	-0.019131
m_1	17.39	16.298	13.989	12.88	14.137
m_2	6.24E-05	0.02768	0.012252	0.0072527	-0.003556
m_3	13.121	6.9488	3.7834	3.4361	3.1995
R	0.99993	0.99998	0.99996	0.99992	0.99997
(e) $y_o = m V$ **for** $|y_o| < 5$ **mm**					
m	18.49	16.96	14.55	13.55	14.62

Table 3. Polynomial coefficients for Q_x/Q_s vs x_o ($|x_o|$ < 15 mm for y_o = 0 and 5 mm, and $|x_o|$ < 10 mm for y_o = 10 and 15 mm) and their inversions up to the fifth and third orders. R-values indicate the reliability of the curve fits. The linear coefficients within $|x_o|$ < 5 mm are listed in the last row.

(a) $H = N_o + N_1 x_o + N_2 x_o^2 + \text{---} + N_5 x_o^5$, ($H = Q_x/Q_s$)				
	$y_o = 0$	**$y_o = 5$**	**$y_o = 10$**	**$y_o = 15$**
N_o	3.20E-05	-0.000551	-0.001332	-0.002377
N_1	0.057954	0.065643	0.089754	0.12658
N_2	-1.14E-07	4.91E-06	1.49E-05	3.21E-05
N_3	-9.89E-05	-0.000129	-0.000268	-0.000516
N_4	2.08E-10	-9.96E-09	-5.15E-08	-1.22E-07
N_5	1.21E-07	1.66E-07	5.64E-07	1.15E-06
R	1	1	1	1
(b) $H = N_o + N_1 x_o + N_2 x_o^2 + N_3 x_o^3$				
N_o	3.11E-05	-0.000507	-0.001285	-0.002267
N_1	0.05645	0.063576	0.088347	0.12371
N_2	-7.33E-08	2.96E-06	1.04E-05	2.14E-05
N_3	-6.82E-05	-8.66E-05	-0.000204	-0.000385
R	0.99996	0.99994	0.99999	0.99997
(c) $x_o = n_o + n_1 H + n_2 H^2 + \text{---} + n_5 H^5$, (Inverted coefficients)				
	$y_o = 0$	**$y_o = 5$**	**$y_o = 10$**	**$y_o = 15$**
n_o	-0.000551	0.0081524	0.014706	0.018208
n_1	17.462	15.597	11.248	8.2602
n_2	-0.000259	0.0036981	0.0001707	0.0083058
n_3	4.4509	0.88597	2.4051	-1.1738
n_4	-0.000822	-0.057578	-0.024826	-0.021612
n_5	30.068	29.088	9.7406	7.1476
R	1	0.99999	1	0.99997
(d) $x_o = n_o + n_1 H + n_2 H^2 + n_3 H^3$				
n_o	-0.000558	0.0094429	0.015501	0.020148
n_1	16.15	13.846	10.645	7.0779
n_2	-0.000341	-0.020362	-0.012441	-0.009957
n_3	18.474	16.789	7.8307	5.3098
R	0.9999	0.99979	0.99994	0.99964
(e) $x_o = n H$ for for $\lvert x_o \rvert$ < 5 mm				
n	17.68	15.67	11.67	8.42

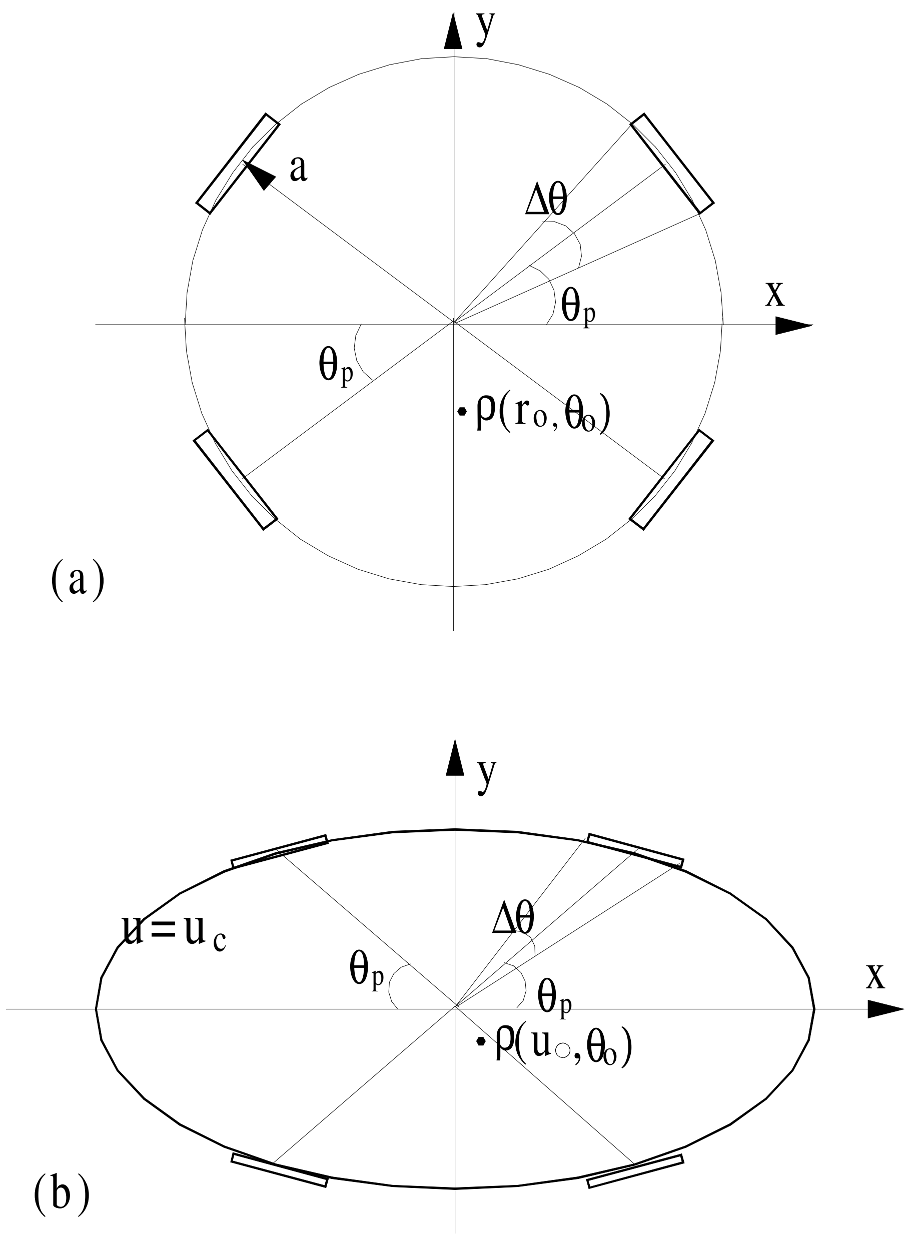

Fig. 1. (a) Four-button BPMs on a circular beam chamber of radius a. Here (a, θ_p) is the button position in the first quadrant, (a $\Delta\theta$) is the button diameter, and (r_o, θ_o) is the beam position. (b) Elliptical beam chamber with major and minor radii of d cosh u_c and d sinh u_c, and foci at $\pm\, d$. (u_c, θ_p) is the four-button BPM position in the first quadrant, (u_c $\Delta\theta$) is the button diameter, and (u_o, θ_o) is the beam position.

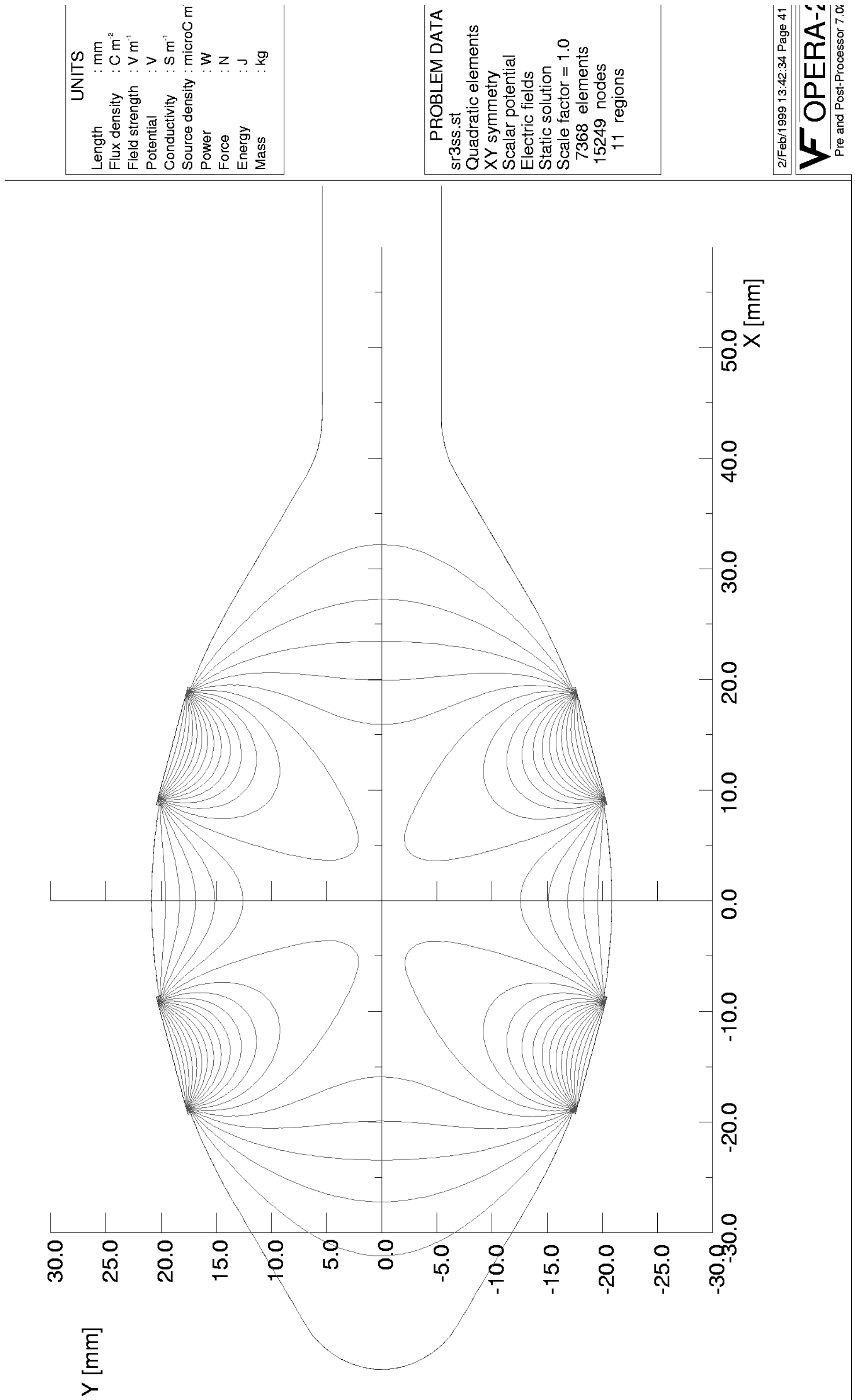

Fig.2. Equipotential lines for sum signals from four-button BPMs installed on the storage ring beam chamber. The 10-mm-diameter buttons are located at (±14.0 mm, ±19.0 mm) flush with the chamber surface. There are 20 equipotential lines between the BPMs (which were applied +1.0 V) and the grounded beam chamber.

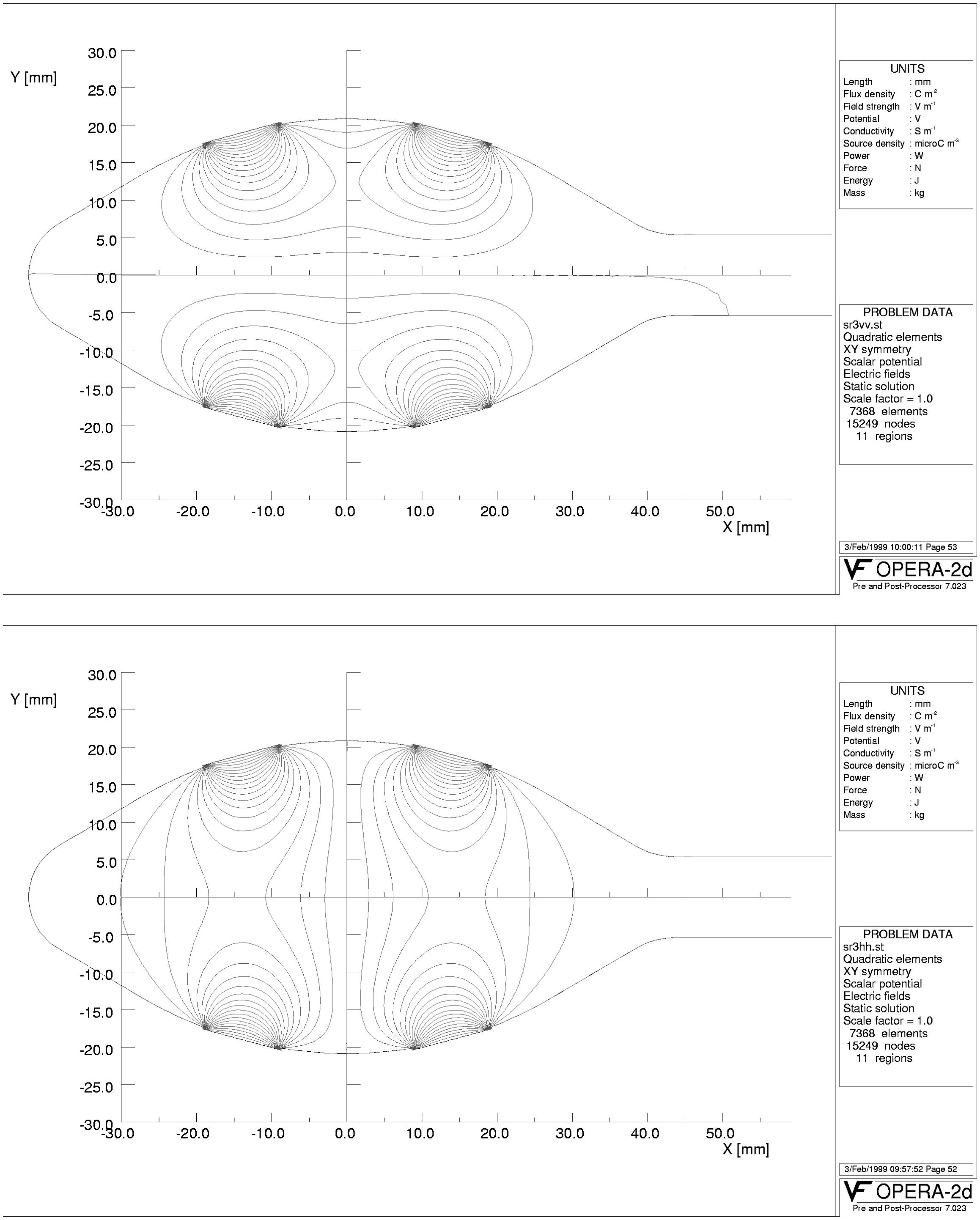

Fig. 3. Top: Forty equipotential lines for vertical signals between the top two BPMs at +1.0 V and bottom two at –1.0 V. Bottom: Forty equipotential lines for horizontal signals between the right two BPMs at +1.0 V and the left two at –1.0 V.

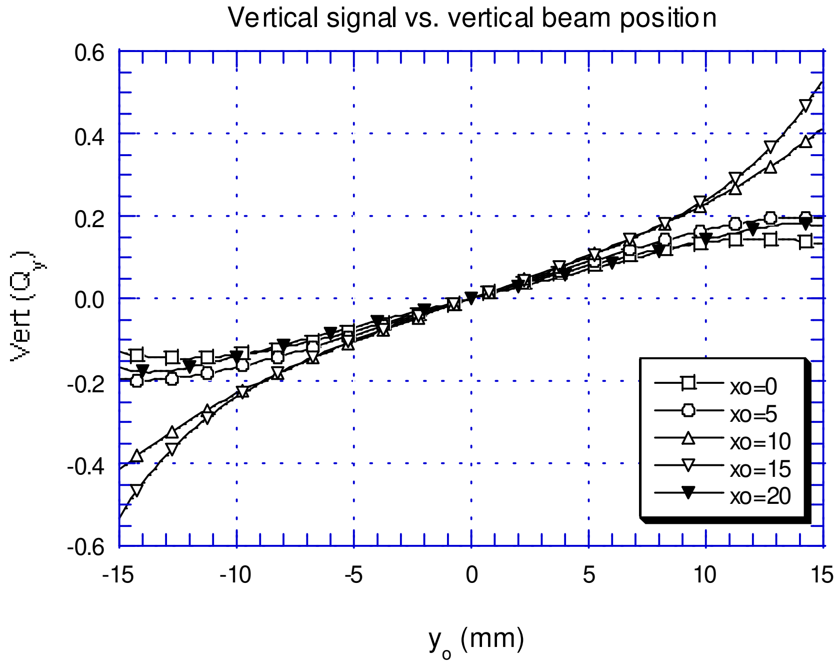

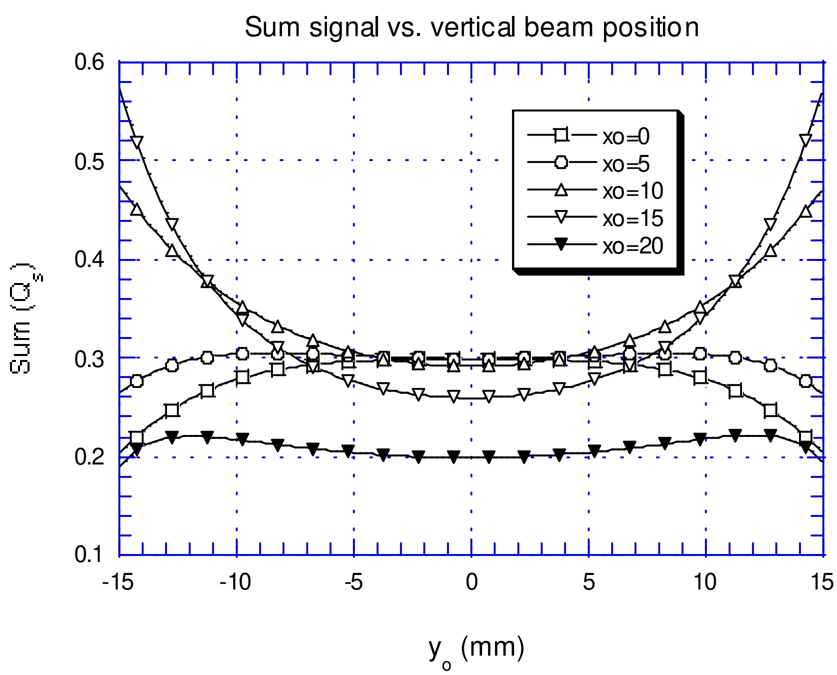

Fig. 4. Vertical (Q_y) (top) and sum (Q_s) (bottom) signals vs vertical beam position y_o at selected horizontal beam positions. The signal units are in volts when the BPMs are applied plus or minus one volt.

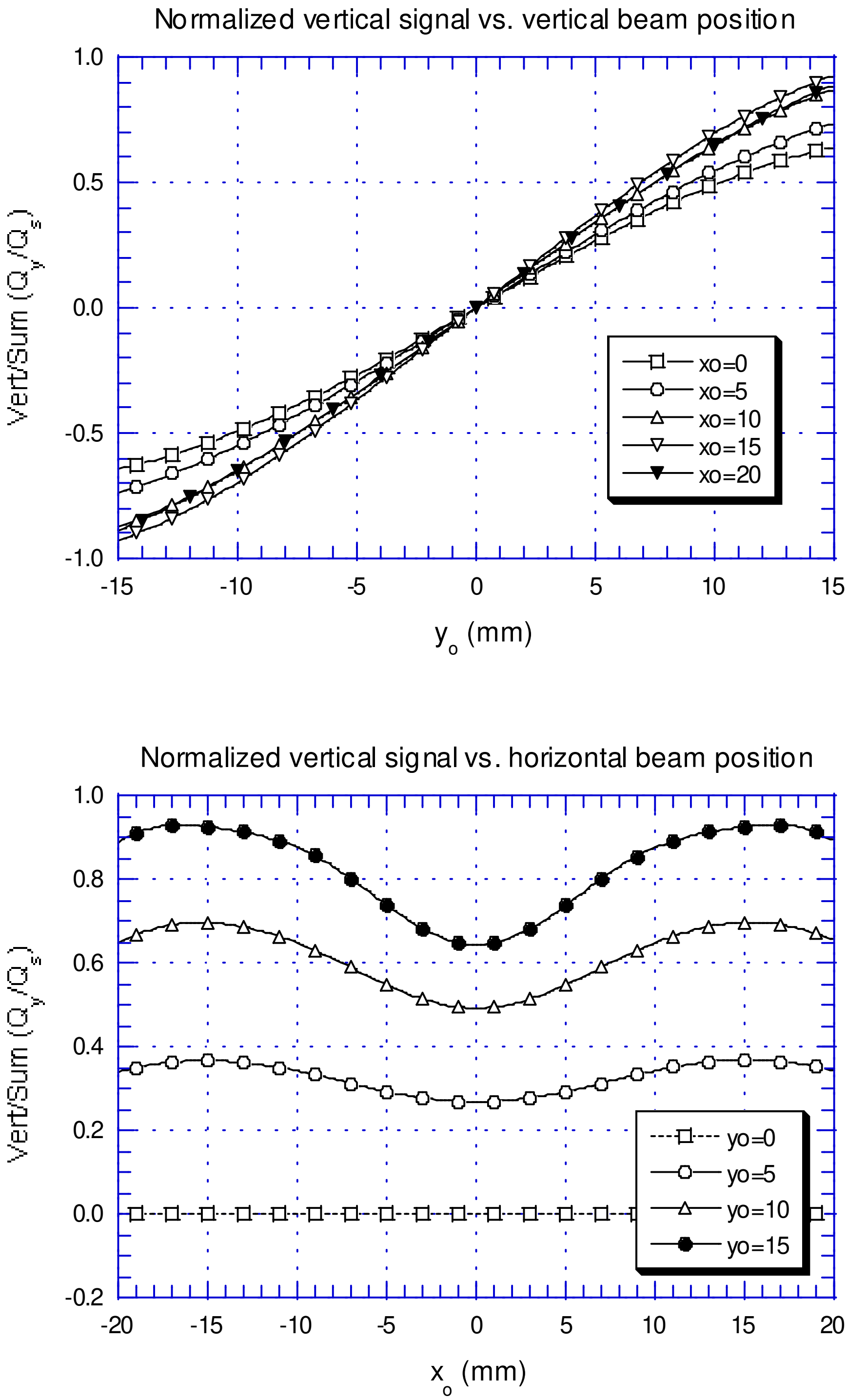

Fig. 5. Normalized vertical signal (Q_y/Q_s) vs vertical beam position (top) and horizontal beam position (bottom).

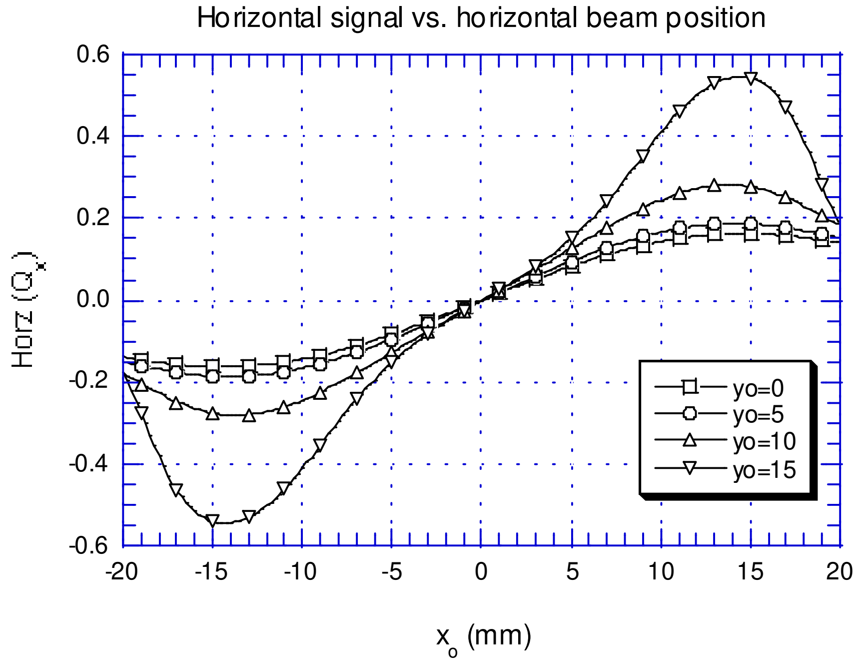

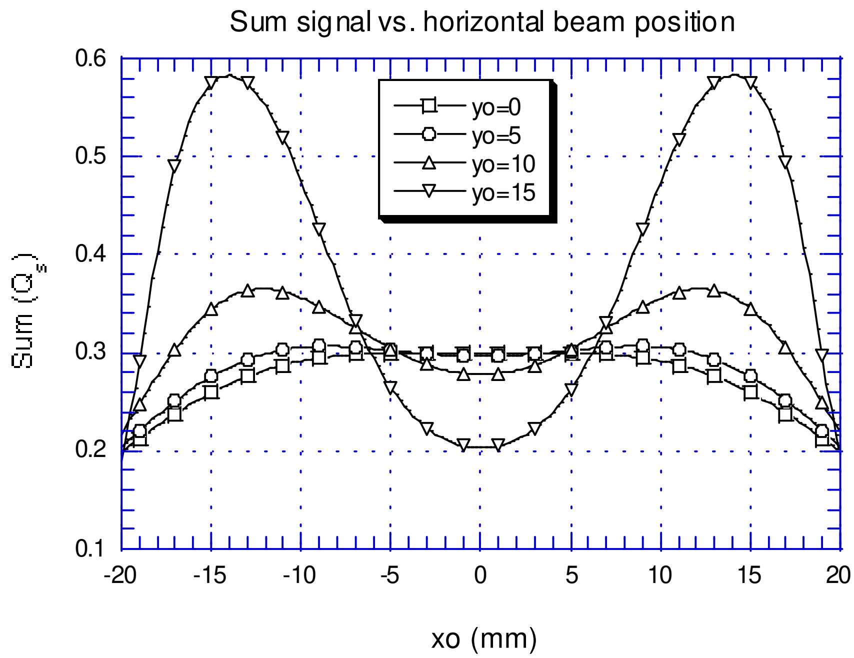

Fig. 6. Horizontal (Q_x) (top) and sum (Q_s) (bottom) signals vs horizontal beam position x_o at selected vertical beam positions. The signal units are in volts when the BPMs are applied plus or minus one volt.

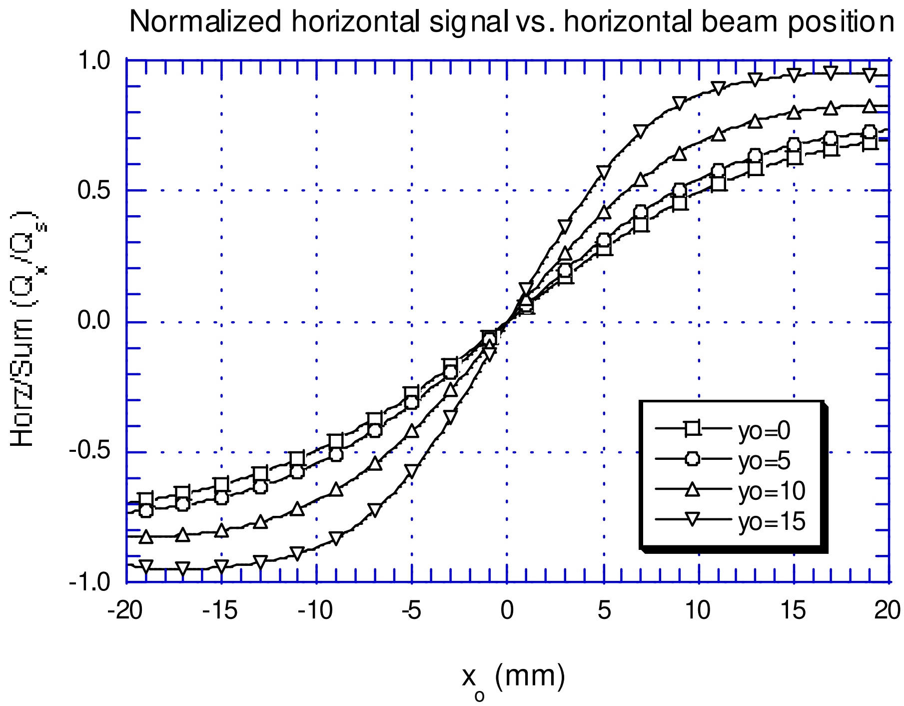

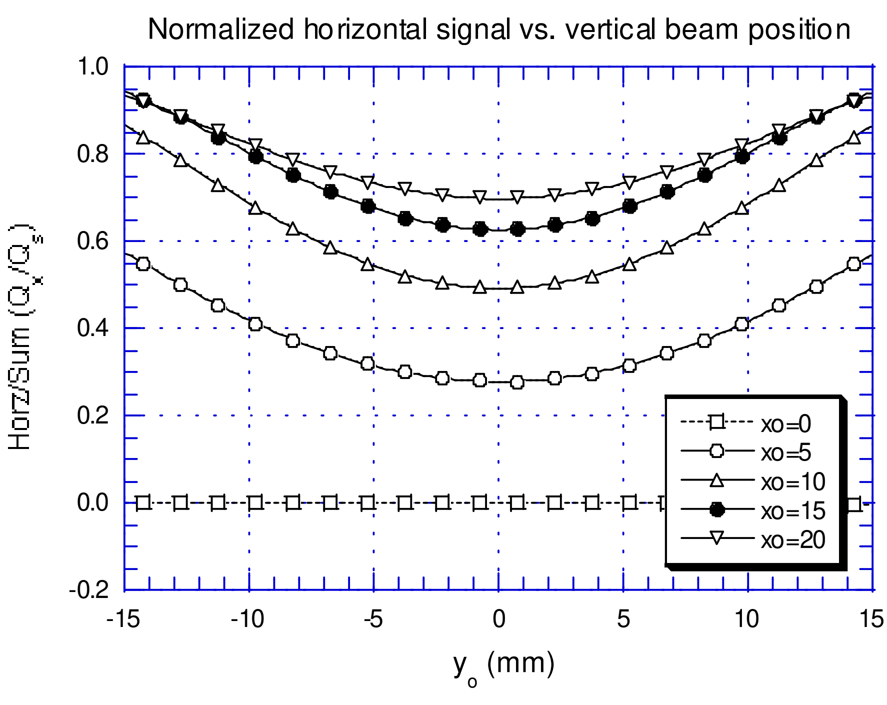

Fig. 7. Normalized horizontal signal (Q_x/Q_s) vs horizontal beam position (top) and vertical beam position (bottom).